Dissolution of Particles in Binary Alloys: Part I. Computer Simulations

ULF H. TUNDAL and NILS RYUM

A detailed numerical study has been made of the dissolution kinetics of particles in binary alloys during isothermal annealing. In earlier models, the assumption was made that the dissolution reaction could be described by the dissolution of only one particle in an infinite matrix or the dissolution of a regular array of particles of equal size. This assumption has been relaxed and a log-normal size distribution of particles has been introduced instead. The calculations have been done numerically by applying a finite difference technique to a spherical particle in a spherical cell of finite size. The presence of a size distribution of particles was found to have a great effect on the dissolution kinetics and, therefore, must be included in a reliable model for the dissolution of particles. The results have been presented in diagrams, giving the volume fraction as a function of the dimensionless annealing time with the geometrical standard deviation as a parameter, and thus should be useful in making accurate predictions of the dissolution kinetics of binary alloys. The curves can be used for all volume fractions provided that all of the particles can be dissolved completely at the temperature considered. Also, equations have been derived that can easily be used to give an estimate of the annealing time to dissolve 90 pct of the initial volume fraction.

I. INTRODUCTION

HOMOGENIZATION and solution heat treatments are very important heat-treatment operations carried out during metal processing. Homogenization is the commonly used term for the treatment resulting in a decrease of the microsegregation formed during solidification, while solution heat treatment refers to the treatment where second-phase particles become unstable and dissolve into the matrix phase. Very often these two processes take place simultaneously, and this is probably the reason for a somewhat inconsistent phrasing in the literature. It is also quite common to use the term homogenization as a general term for high-temperature annealing of castings. This is also inadequate, because a heterogenization instead of a homogenization occurs quite often during high-temperature annealing. The term soaking is an appropriate term for such high-temperature annealing.

In spite of their obvious industrial importance, the homogenization and solution heat-treatment reactions have received rather limited scientific attention. On the other hand, the reverse reaction, namely the nucleation and growth of second-phase particles in a homogeneous supersaturated solution, has been under extensive investigation for a long time. The reason for this difference in scientific interest probably reflects the difference in the central problems in the two cases. For the latter reaction, the central problem is related to the physics of the reactions (nucleation and growth), while for the former reaction, the central problem is related to the complexity of the mathematical description.

ULF H. TUNDAL, Research Scientist, is with the Division of Metallurgy, SINTEF, N-7034 Trondheim, Norway. NILS RYUM, Professor, is with the Department of Metallurgy, The Norwegian Institute of Technology, N-7034 Trondheim, Norway.

Manuscript submitted April 10, 1991.

The first attempt to develop mathematical models for diffusion-controlled dissolution of second-phase particles in binary alloys was made by Thomas and Whelan,[1] Aaron,[2] and Whelan.[3] These early models were limited to the dissolution of one single particle in an infinite matrix. Thomas and Whelan approximated the dissolution process to the reverse growth process, while Aaron's model was a one-dimensional model and thus cannot describe the dissolution of small particles. Whelan derived the correct differential equation for the dissolution of a spherical particle in an infinite matrix and also gave the general solution to this equation. The dissolution process was found to be much more complicated to describe mathematically than the growth process (or the reversed growth process). Whelan also discussed some limiting cases where the solution could be given in closed forms.

In all of these early attempts to describe the dissolution process mathematically, several assumptions were made.

(1) The rate of dissolution is limited by long-range diffusion; hence, equilibrium is always established at the interface between the particle and the matrix.
(2) The diffusion coefficient D is independent of the concentration.
(3) The stationary interface approximation is used to obtain the concentration gradient in the matrix.

These approximations are needed to obtain solutions in closed forms. The validity of approximations 1 and 2 is related to the thermodynamics of the alloy and in principle can be checked experimentally. In the stationary interface approximation, the concentration profile outside a particle of radius R is the same as that which exists if the particle has been fixed at R from the start of the dissolution process. However, when a particle dissolves, the interface moves away from the matrix. This means that the concentration gradients calculated by the stationary interface assumption are too steep at all times

and particularly when R approaches zero. This approximation is a reasonable one when a solute-rich particle is dissolving in a dilute matrix.

Aaron and Kotler[4] have studied the thermodynamical effect of curvature on the dissolution kinetics. The influence of curvature they found is negligible unless the difference between the solute concentration at the particle/matrix interface $C^{\alpha/\beta}$ and the matrix concentration C_m is sufficiently small. However, the reduction in total dissolution time is considerably less than 10 pct in all practical cases.

In order to describe the dissolution process in real materials, the model must contain the volume fraction of a second phase instead of only one isolated particle. This introduces a topological factor into the dissolution process: the shape and the spatial distribution of the second phase. Only some special cases can now be treated analytically. Nolfi *et al.*[5,6,7] studied the dissolution of spherical particles of equal size arranged in a simple cubic lattice and solved the diffusion equation by a series expansion. A consequence of this type of modeling is that all of the particles dissolve at the same rate.

Singh and Flemings[8,9] studied the dissolution of interdendritic second-phase particles in a cast structure by assuming the particles to be plate-shaped and arranged in parallel, thus reducing the diffusion to linear diffusion. In this way, they also obtained an analytic expression for the dissolution process. Refinements of this model have been carried out by Singh *et al.*[10] and Fuchs and Roósz.[11] These refinements, however, result in equations that can be solved only by numerical methods.

A rather ambitious application of the numerical solution methods of the dissolution process was carried out by Tanzilli and Heckel.[12] They solved the diffusion equation numerically using a finite difference technique. Their model in principle can be used to describe the dissolution kinetics in materials with a given volume fraction of precipitates of different shapes. However, their model has some severe limitations. The salient assumptions in the model are that all precipitates are of equal size and that they are divided into identical, spherical cells having the particle at their center. A consequence of this is that all of the precipitates dissolve completely at the same annealing time.

Ågren[13] has developed a model similar to that of Tanzilli *et al.* but extended it also to cover diffusion in multicomponent alloys. He also demonstrated convincingly the applicability of this model to a number of diffusional reactions in steels.[14–18] In principle, the model is also applicable to other alloys.

Baty *et al.*[19] presented a method for predicting the variation with time of the particle size distribution by assuming that the size distribution does not change shape during the annealing process. The assumption that the particle distribution is moving rigidly to the left is not well founded. This implies that the radius of a large particle decreases at the same rate as a small particle, which is not correct. Also, they did not include the volume fraction of particles in this model so the method is thus of limited use.

The analytical and numerical approaches referred to above are not well suited for solving problems related to industrial practice. In general, one has to carry out additional extensive computer calculations to obtain useful results. The intention of the present work is to present the results in such a way that results can be obtained directly from nomogrames without additional calculations. Also, the assumption in earlier treatments of equal size of all particles is relaxed, and a particle size distribution is included instead.

II. ANALYSIS

The main intention of the present investigation is to relax the assumption used in earlier investigations that all particles are of equal size and to introduce a particle size distribution instead. When the particles are assumed to be all of equal size, it is reasonable to arrange the particle in space in a simple, regular manner, as done, for instance, by Nolfi *et al.*[5] With a particle size distribution present, the arrangement of the particles in space needs some consideration. It is convenient to discuss two limiting cases.

A. *Model 1*

When all of the particles are nucleated simultaneously in a uniform, supersaturated solid solution, the particles will grow independently of each other until soft impingement occurs. As a first approximation, each particle is surrounded by a solute-depleted cell with a size proportional to the size of the particle. This approximation is assumed to be valid as long as extensive coarsening has not taken place. The above arguments lead to our Model 1: the material is divided into spherical cells with a size distribution that matches the size distribution of the particles. Each particle is located in the center of the corresponding cell. The size of the cells is such that the concentration of solute atoms (including the particle) is the same in all cells and equal to C_0. Figure 1 gives a two-dimensional (2-D) picture of the particle/cell arrangement. For further discussions about the assumptions in Model 1, the reader is referred to Appendix A.

In order to use the model on a real material, one has to know the particle size distribution in space. This can be obtained by the Schwartz-Saltykov analysis, as described by Underwood,[20] which gives the size distribution of spheres in space from a particle size distribution in a planar section. Because the volume fraction of particles in each class is known at the start of the dissolution

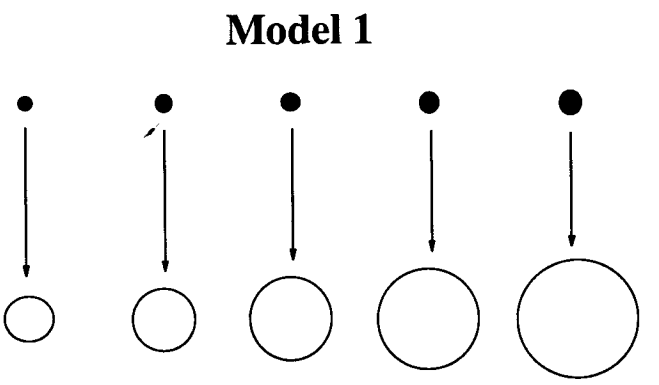

Fig. 1—Schematic 2-D diagram of the particle/cell arrangement in Model 1.

process, the total volume fraction of particles in the alloy as a function of dissolution time can be calculated.

B. *Model 2*

As coarsening proceeds, the simple correspondence between the particle size and the cell size is gradually lost. For instance, when one particular particle has dissolved completely during the coarsening process, its corresponding cell volume is then included in the neighboring cells, and in the extreme case, there will be no simple correspondence between the particle size and the cell size. In Model 2, we retain the assumption that initially the size distributions of the particles and the cells have the same shape, but there is no correspondence between the size of the particles and the size of the cells. This model is shown schematically in Figure 2. The particles from each size class are randomly distributed in cells of different sizes. There are in total $(NC)^2$ (NC = number of size classes) different particle/cell systems, and the computing time thus increases rapidly with increasing number of size classes. The average concentration in the material is C_0, but contrary to Model 1, the average concentration in the different cells will vary in Model 2.

It is obvious that the smallest particles in the largest cells will have the shortest dissolution times. When the particles in one system (*i.e.*, particles of one particular size in cells of one particular size) have dissolved, the volume and mass from this system are transferred to all of the other systems. The volume of the cells and the total mass of the solute elements are then added equally to the remaining cells as shells outside existing cells. The solution concentration in the transferred volume is taken as the average concentration in this particular cell. The volume of an existing cell will thus increase as the particles are dissolving. When few particles are left, each particle will have a large volume to dissolve into, but the solute concentration in this volume has also increased and the dissolution process is thus slowed down. A large particle in a small cell may temporarily stop dissolving, because the cell is saturated with solute. However, when other particles have dissolved, the volume of this cell will increase and the particle will again start to dissolve. This method of distributing particles among the different cells is meant to simulate the situation that some particles are clustered together and that the dissolution process in these clustered regions is slowed down relatively more than in other regions of the material.

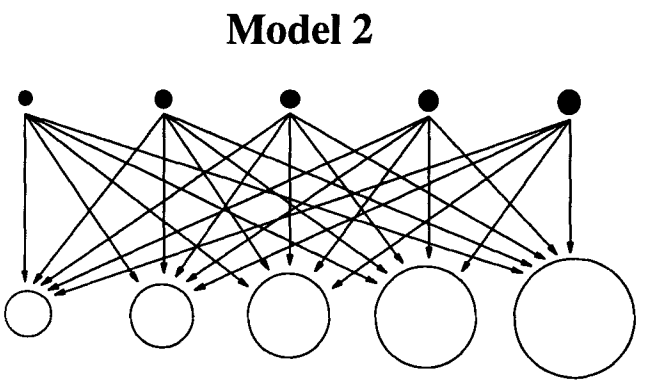

Fig. 2—Schematic 2-D diagram of the particle/cell arrangement in Model 2.

An essential part of both Models 1 and 2 is the calculation of the rate of dissolution of one spherical particle in the center of a spherical cell. The calculation is done numerically by a method that closely follows the methods described by Patankar[21] and is given in some detail in Appendix B. For convenience, assumptions 1 and 2 in Section I are used in these calculations. The introduction of a concentration-dependent diffusion coefficient and a nonequilibrium, time-dependent interface concentration would cause no major computational problems. Assumption 3 is relaxed and the moving interface solution is applied instead, as explained in Appendix B. Because of the small influence of curvature of the particles on the dissolution kinetics, the effect is not included in the calculations. Finally, the chemical composition of the particle is assumed to be the same at all temperatures, thus no diffusion occurs within the particle. The temperature dependence of the composition of intermetallic phases is small for many binary systems so this is a reasonable assumption.

III. RESULTS

Before presenting the results, it is necessary to define the parameters used in the equations presented subsequently.

In the theory of the diffusion-controlled rate of growth of an isolated particle in a supersaturated solid solution, the growth rate dR/dt can be expressed in the following simple way:

$$\frac{dR}{dt} = 2\alpha^2\left(\frac{D}{R}\right) \qquad [1]$$

where α, often referred to as the growth constant, is a function of the relevant concentration of the diffusion field. It is convenient to write

$$\alpha = \alpha(k) \qquad [2]$$

where

$$k = \frac{C^{\alpha/\beta} - C_m}{\bar{C}^{\beta/\alpha} - C^{\alpha/\beta}} \qquad [3]$$

where the different concentrations are defined in Figures 3(a) and (b) and $\bar{C}^{\beta/\alpha} = C^{\beta/\alpha}(V_m^\alpha/V_m^\beta)$. A small value of k means that the concentration of B atoms in the particle is so large compared to the solubility of B atoms in the matrix that atoms can diffuse away from the particle without causing a rapid movement of the particle/matrix interface. As shown by Whelan,[3] the rate of dissolution of a spherical particle in an infinite matrix under the stationary interface approximation can be written in the following way:

$$\frac{dR}{dt} = -k\frac{D}{R} - k\sqrt{\frac{D}{\pi t}} \qquad [4]$$

The first term on the right-hand side of this equation arises from the part of the concentration field which gives the dissolution rate as the reverse of the growth rate. This

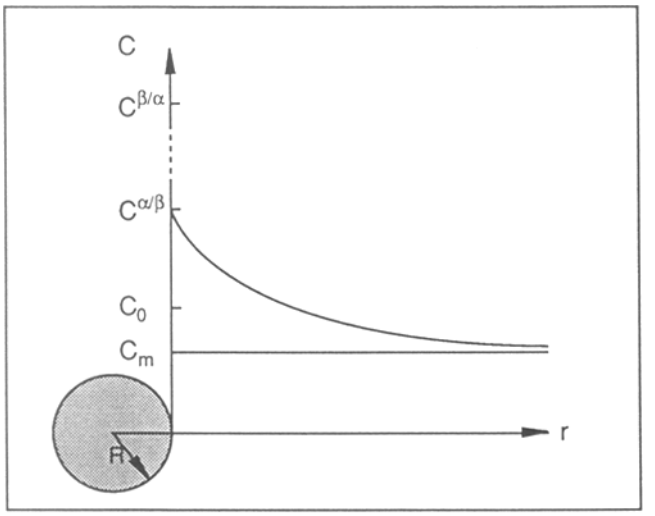

(*a*)

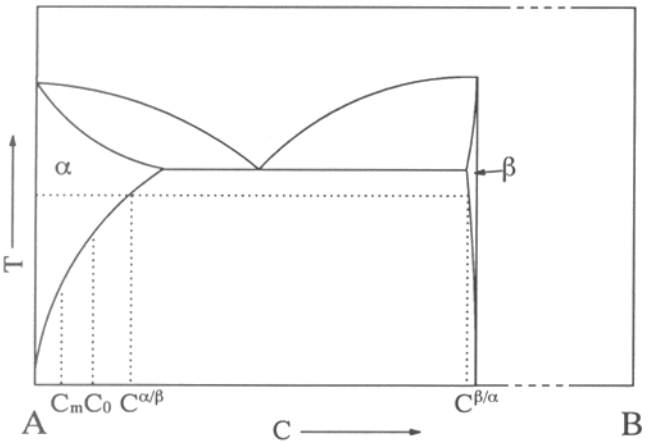

(*b*)

Fig. 3—(*a*) Schematic diagram of the solute concentration in the vicinity of a dissolving particle initially in equilibrium with the matrix. (*b*) Schematic binary phase diagram.

part of the field is referred to by Whelan as the steady-state part. The second term on the right-hand side of Eq. [4] is seen to decrease with increasing dissolution time, and the corresponding part of the concentration field is referred to as the transient part. The value of k is also a measure of the effect of the transient part on the dissolution process. For small values of k, the dissolution process is dominated by the stationary part, while for larger values, the transient part is more important. Large values of k mean that the solubility of B atoms in the matrix is comparable to the concentration of B atoms in the particle. This means that a large part of the particle can be dissolved before the B atoms have to diffuse a long distance away from the particle.

When an alloy containing many particles is considered, the volume fraction of the particles must appear as a parameter in the rate of dissolution. However, instead of introducing the volume fraction as this characterizing parameter, it is more convenient to introduce the parameter

$$b = \frac{C_0 - C_m}{C^{\alpha/\beta} - C_m} \qquad [5]$$

The value of b varies from 0 to 1. When $b = 0$, *i.e.*, $C_0 = C_m$, the volume fraction is zero. This is the case discussed by Whelan. When $b = 1$, *i.e.*, $C_0 = C^{\alpha/\beta}$, the alloy contains the maximum volume fraction of particles that can be dissolved at the temperature considered.

The dissolution time t is normalized against the dissolution time t_0 for a particle of size R^0 dissolving in an infinite matrix.

$$t_0 = \frac{(R^0)^2}{2Dk} \qquad [6]$$

thus the normalized time τ becomes

$$\tau = \frac{2Dkt}{(R^0)^2} \qquad [7]$$

A. *Dissolution of One Particle*

In all of the results presented in this investigation, the movement of the particle/matrix interface is included in the calculations. In Figure 4, a comparison is made between the concentration field calculated by this method and the stationary interface approximation. In Figure 4(a), the concentration profiles are shown for $k = 0.01$ and $b \approx 0$. This means that the stationary part of the concentration field is dominating and that the solute atoms can diffuse away from the particle without causing a rapid movement of the interface. As can be seen, in the early stage of the dissolution process, the concentration profiles predicted by the stationary interface approximation coincide rather well with profiles predicted by our model, in which the movement of the interface is included. When the radius of the particle approaches zero, the deviation increases. In Figure 4(b), $k = 0.25$ and $b \approx 0$, the difference between the profiles predicted by the stationary interface approximation and our model is considerable even at short dissolution times.

Following Whelan, we have plotted the variation of $\rho^2 = (R/R^0)^2$ with annealing time τ for different values of b, as shown in Figure 5. The time τ^* to dissolve the particle completely increases with increasing b. The reason for this is as follows: the average concentration of solute atoms in the matrix increases with the increasing value of b. This means an increasing tendency for a buildup of solute atoms close to the dissolving particle. The rate of dissolution is thus slowed down, particularly when the radius approaches zero. The effect of the transient part of the concentration field is also evident from Figure 5. When $k = 0.25$ (Figure 5(b)), the curvature of the curves is more pronounced than when $k = 0.01$ (Figure 5(a)). This can easily be seen when comparing the curves for $b = 0.01$ in the two cases.

In Figure 6, the time τ^* needed to dissolve the particle completely is plotted against b for different values of k. As can be seen, when b approaches unity, τ^* approaches infinity. Because k is included in the normalized time τ, the differences in the curves are only due to the effect of the transient part of the dissolution process, which is more pronounced for large values of k.

B. *Dissolution of an Assembly of Particles—Model 1*

The input to Models 1 and 2 is the distribution of particles in space. The Schwartz-Saltykov analysis gives the

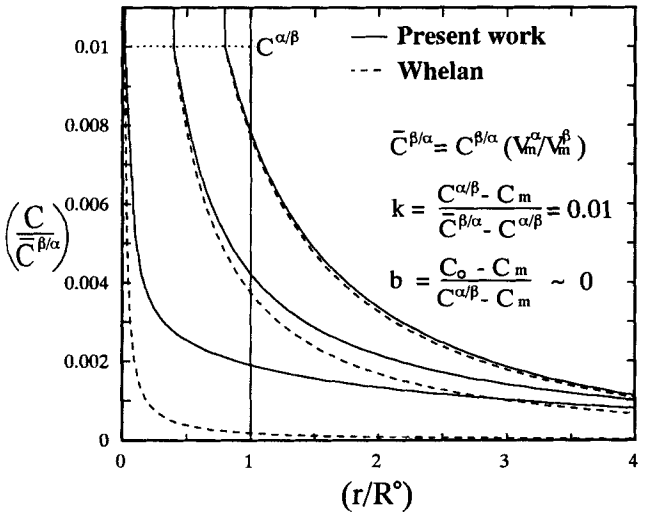

(a)

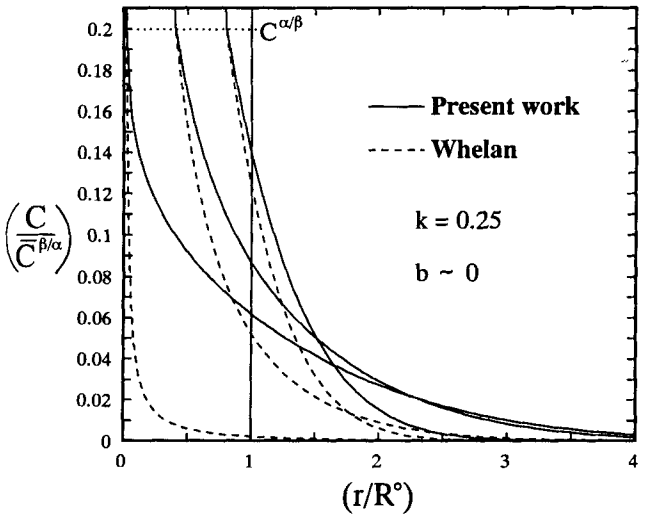

(b)

Fig. 4—(*a*) and (*b*) Concentration profiles in the vicinity of a spherical particle predicted by the stationary interface approximation and our model, in which the moving interface is included.

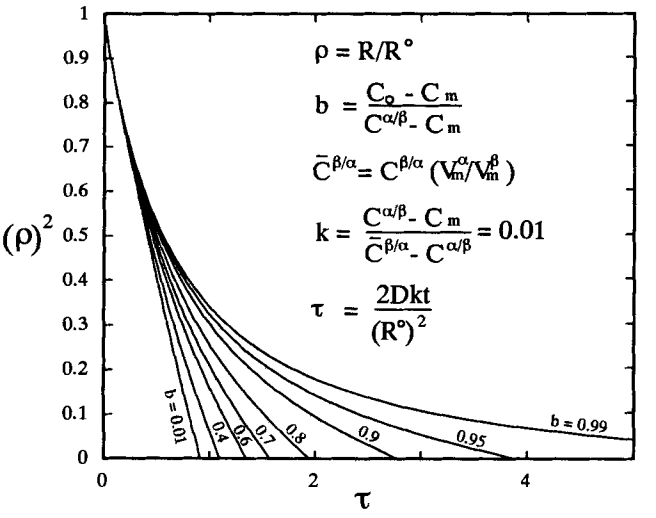

(a)

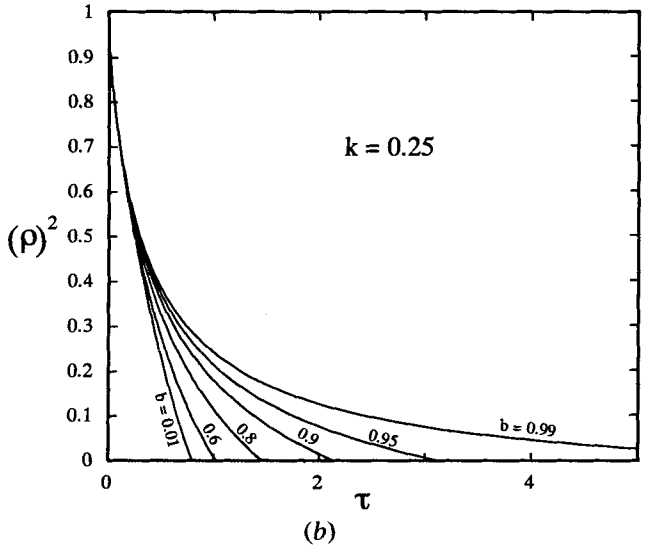

(b)

Fig. 5—(*a*) and (*b*) The variation of $\rho^2 = (R/R^0)^2$ with annealing time τ plotted for different values of b and two values of k.

number of particles in size classes from measurements on a metallographic specimen. These data can be put directly into the models. However, in order to present our results in such a way that practical applications are easily obtained, a type of standardized particle size distributions has to be used. The log-normal distribution is one of the most frequently observed distributions of small particles, and our results are presented for this type of particle size distribution. The log-normal size distribution can be written in the following way:

$$y(R) = \frac{1}{R \ln \sigma_g \sqrt{2\pi}} \exp\left(-\frac{(\ln R - \ln \bar{R}_g)^2}{2(\ln \sigma_g)^2}\right) \quad [8]$$

with

$$\bar{R}_a = \bar{R}_g \exp\left(\frac{(\ln \sigma_g)^2}{2}\right) \quad [9]$$

where R is the radius of the particle, σ_g is the geometric standard deviation of the distribution, and $\bar{R}_g$ and $\bar{R}_a$ are

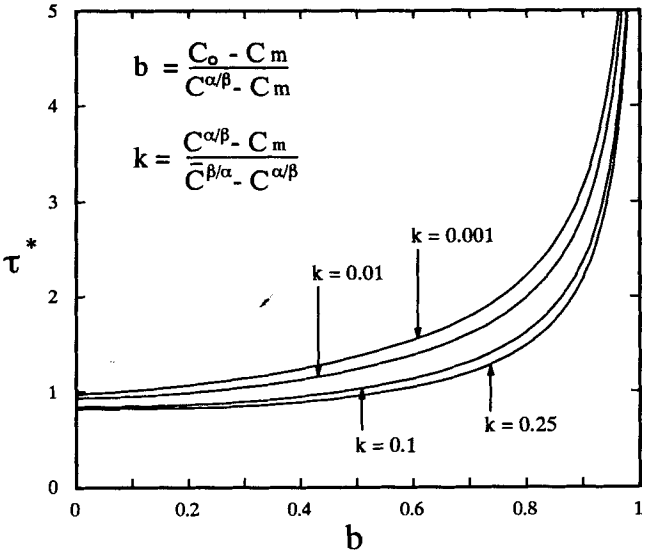

Fig. 6—The time τ^* needed to dissolve a particle completely plotted as a function of b for different values of k.

the geometric and arithmetic means, respectively. In practice, a convenient way to check whether an experimental particle distribution matches a log-normal distribution is to plot the cumulative frequency in a probability paper with logarithmic size axes, as described by Exner.[22] If this plot gives a line that is roughly straight, the size distribution is approximately log-normal and our diagrams are applicable.

The size distribution of the particles is described by a continuous function. The numerical calculations are, of course, limited to a finite number of particles distributed among different size classes. This requires upper and lower limits for the particle sizes in the distributions. These limits were decided by requiring 99 pct of the number of particles to be within these limits. This cutoff is similar to obtaining an experimental size distribution, and the error introduced is thus negligible.

Since k is included in the normalized time τ, the differences in the curves in Figure 6 are moderate for a wide range of k values. The same was found to be the case for the dissolution kinetics of an assembly of particles. Thus, all calculations have been made with $k = 0.01$. However, for other k values, one can still use the curves, but the values of τ have to be corrected if more precise estimates of the volume fraction as a function of time τ are needed. A more correct value of the time τ becomes

$$\tau_c = \left(\frac{0.01}{k}\right)^{0.05} \tau \qquad [10]$$

where τ is the value read from the curves and τ_c is the corrected value. This correction makes the curves valid for all k values.

In Figures 7(a) through (d), the relative volume fraction of particles f/f^0 is plotted as a function of time τ for four different values of b and a range of different values of σ_g in the interval of 1 to 2. Frequently observed σ_g values for distributions of small particles in a planar section are between 1.4 and 1.6 and somewhat smaller when the planar distribution is transferred to a spatial distribution. There is a clear tendency for the dissolution rates to level out at the end of the dissolution process for large b values. This is also illustrated in Figure 8, where the relative volume fraction of particles f/f^0 as a function of time τ is shown for $\sigma_g = 1.5$ and four different values of b. The effect of b on the dissolution kinetics is small for b values less than about 0.4.

In Figures 9(a) and (b), the relative arithmetic mean radius $\bar{\rho}$ as a function of time τ for Model 1 is shown for $b = 0.4$ and $b = 0.99$ for different values of σ_g. For $b = 0.4$, $\bar{\rho}$ first decreases and subsequently increases with time for large values of σ_g. The reason for this is that after a comparatively short time, the smallest particles disappear, thus leading to an increase in the mean radius. For particle size distributions with medium values of σ_g, the mean radius as a function of time is seen to reach a plateau before it decreases to zero. For $b = 0.99$, $\bar{\rho}$ decreases more smoothly with annealing time τ.

C. *Dissolution of an Assembly of Particles—Model 2*

Results obtained by Model 2 are shown in Figures 10(a) and (b). When comparing these results with the corresponding results obtained by Model 1 (Figures 7(a) through (d)), the two models seem to give very similar results. However, a close examination reveals essential differences: in general, Model 2 predicts a lower rate of dissolution than Model 1. This tendency increases with increasing values of b and σ_g, as shown in Figures 11(a) and (b).

IV. DISCUSSION AND CONCLUSIONS

The basis of Model 1 is the assumption that a one to one correspondence exists between the particle sizes and the cell sizes, as shown in Figure 1. In Model 2, on the other hand, this correspondence is completely lost. The two models thus represent two extremes: Model 1 represents the case where no particle coarsening has taken place before dissolution, while Model 2 is introduced to determine an upper limit for the volume fraction as a function of annealing time. Model 2 is thus comparable to the case where extensive coarsening has taken place. Therefore, in practice, the volume fraction as a function of annealing time therefore lies in between the volume fractions predicted by these two models.

In addition, the assumptions are made that each particle is located at the center of the corresponding cell and that the cells are spherical. Neither of these assumptions is strictly correct. This means that our models probably slightly overestimate the dissolution rates. One final assumption in the model is that the particles are all spherical. This seems to be a restrictive assumption, but if the dissolution rate is determined by volume diffusion, the shape of the particles is likely to have a minor influence on the dissolution kinetics. Whelan[3] proposed that the shape of the diffusion field a long distance away from the precipitate is approximately spherical even for a thin disc-like precipitate. The influence of the shape of the particle on the rate of dissolution has also been studied by Brown.[23] He solved the diffusion equation numerically in two dimensions and found that the total dissolution times were the same for circular and square precipitates. He concluded that if the dissolution is controlled by volume diffusion, the precipitates will become spherical as they shrink, and that the dissolution time is the same as for a sphere of equal volume.

The main difficulties related to determining the dissolution rates for particles of irregular shapes are associated with the transformation of the particle distribution obtained in a planar section to a distribution in space. The methods for making such transformations are valid only for spheres or for particles of regular shapes.

As pointed out by Whelan,[3] the transient part of the concentration field has a significant influence on the dissolution time τ^* of a spherical particle in an infinite matrix. This effect is illustrated in Figure 6, with $b \approx 0$. For a very concentrated particle ($k \approx 0$), $\tau^* \approx 1$, while for $k = 0.25$ (equivalent to $p = 0.2$ in the article of Whelan), $\tau^* = 0.82$. Whelan calculated a dissolution time $\tau^* = 0.57$ for the same k value. This difference in dissolution time is due to the stationary interface approximation used by Whelan. He also advances arguments for the correct value of τ^* to be somewhat higher than 0.57. His arguments are supported by our calculations shown in Figure 4(b). For $k = 0.25$ and $b = 0$,

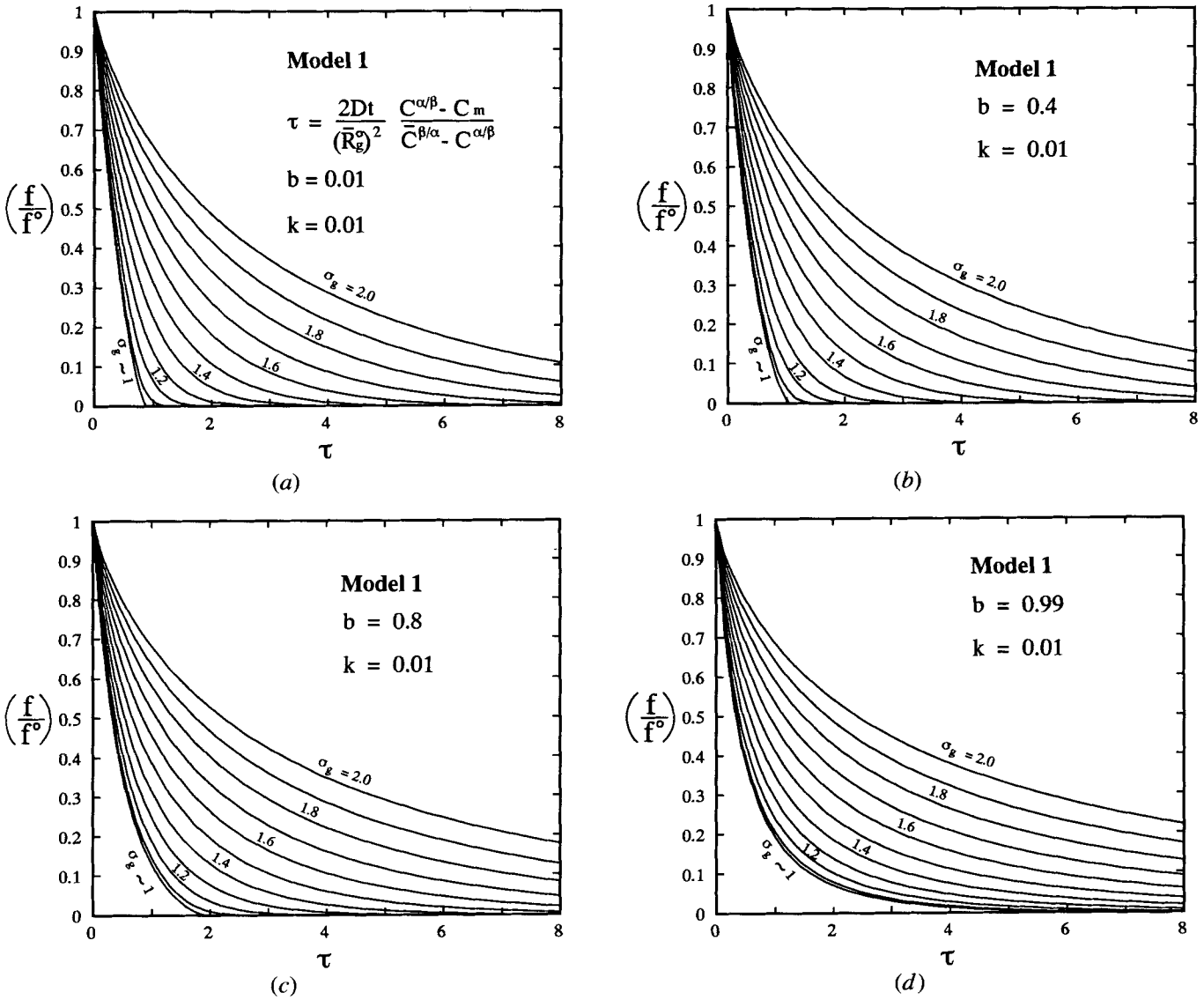

Fig. 7—(*a*) through (*d*) Volume fraction f/f^0 against time τ for four different values of b and a range of different values of σ_g (Model 1).

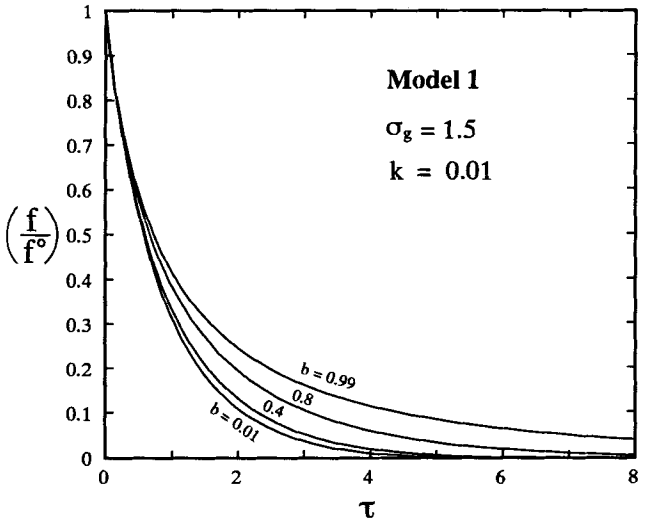

Fig. 8—Effect of b on the dissolution kinetics for a fixed particle size distribution with $\sigma_g = 1.5$.

the stationary interface approximation gives too steep of a concentration gradient at all annealing times and a correspondingly too short dissolution time.

When an estimate of the time τ^* to dissolve one particle completely is sufficient, an acceptable relationship would be the value obtained by curve fitting:

$$\tau^* \approx \left(0.45 + \frac{0.46}{(1-b)^{0.69}}\right)\left(\frac{0.01}{k}\right)^{0.05}$$

$$0 \leq b \leq 0.95 \qquad [11]$$

When the assumption of equal size of the particles is relaxed and a log-normal particle size distribution is introduced in its place, a great effect on the calculated dissolution kinetics is observed.

In Figure 12, the time $\tau_{0.9}$ to dissolve 90 pct of the initial volume fraction of particles is plotted against the geometric standard deviation σ_g of the log-normal distribution. The time τ can be normalized against the arithmetic as well as the geometric mean radius. For a constant

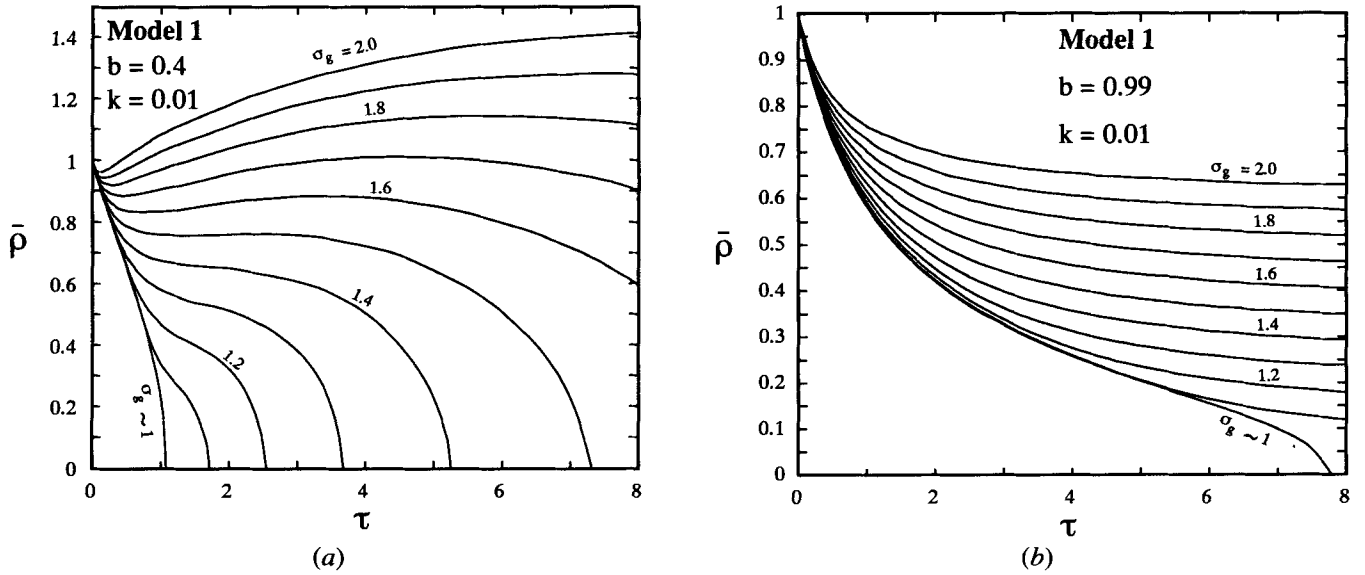

Fig. 9—The relative arithmetic mean radius $\bar{\rho} = \bar{R}_a/\bar{R}_a^0$ as a function of time τ from Model 1 is shown for (*a*) $b = 0.4$ and (*b*) $b = 0.99$ and a range of different values of σ_g.

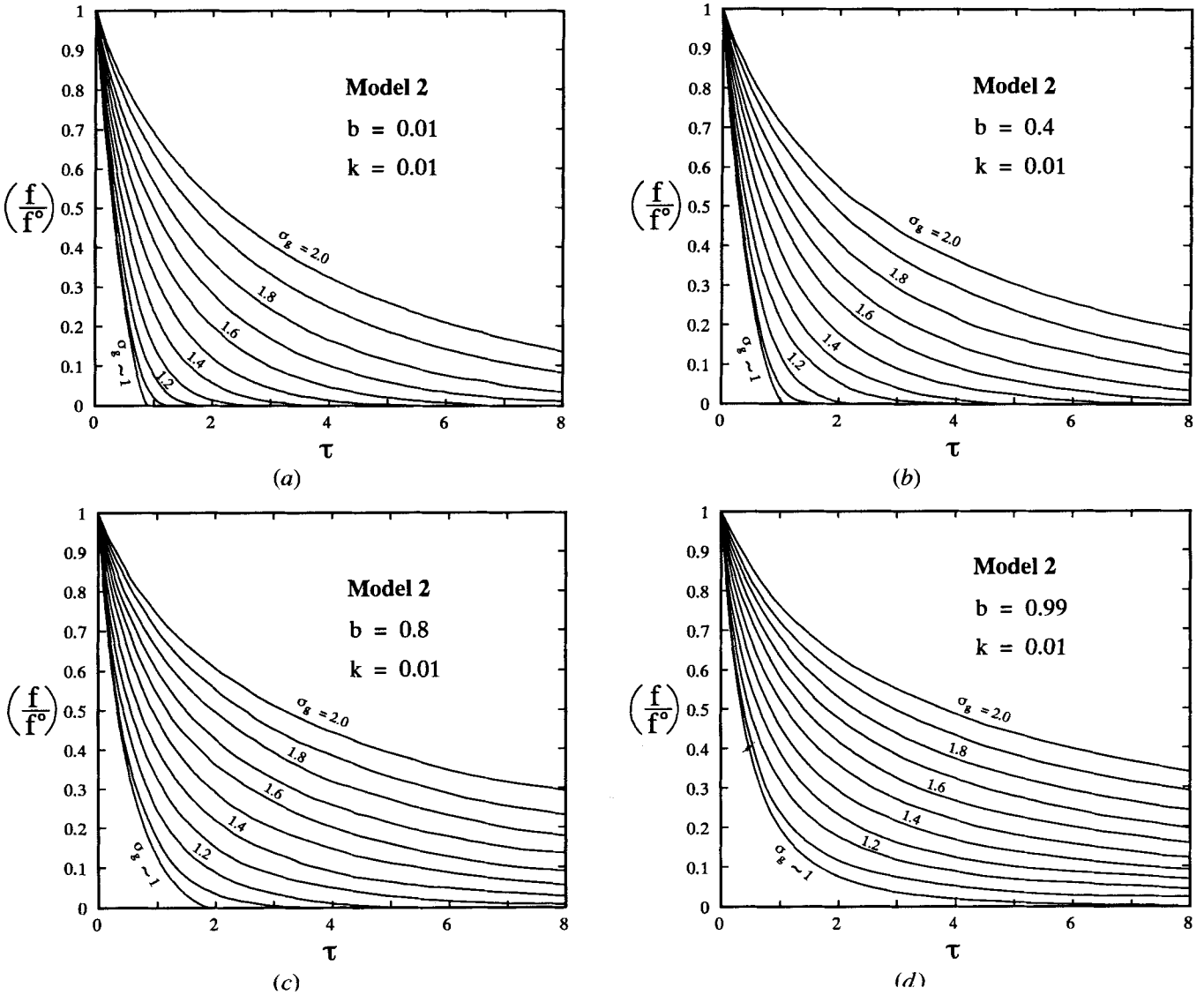

Fig. 10—(*a*) through (*d*) Volume fraction f/f^0 against time τ for four different values of b and a range of different values of σ_g (Model 2).

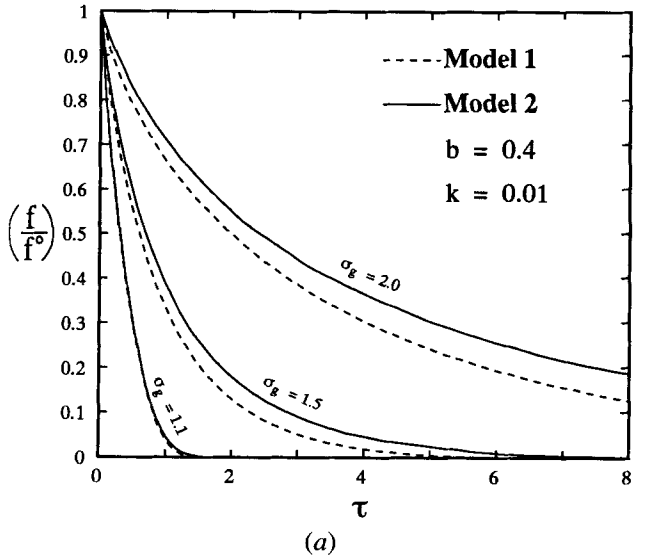

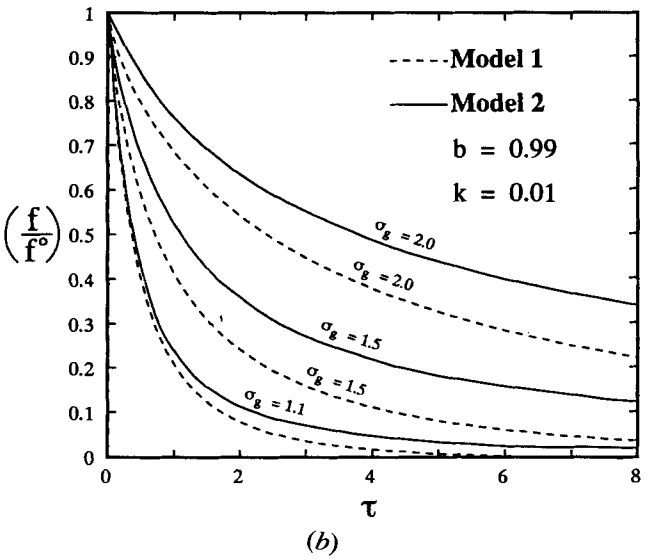

Fig. 11—(*a*) and (*b*) Comparison of the rate of dissolution predicted by Model 1 and Model 2. As can be seen, Model 2 generally predicts lower dissolution rates than Model 1, and the difference is seen to increase with increasing values of b and σ_g.

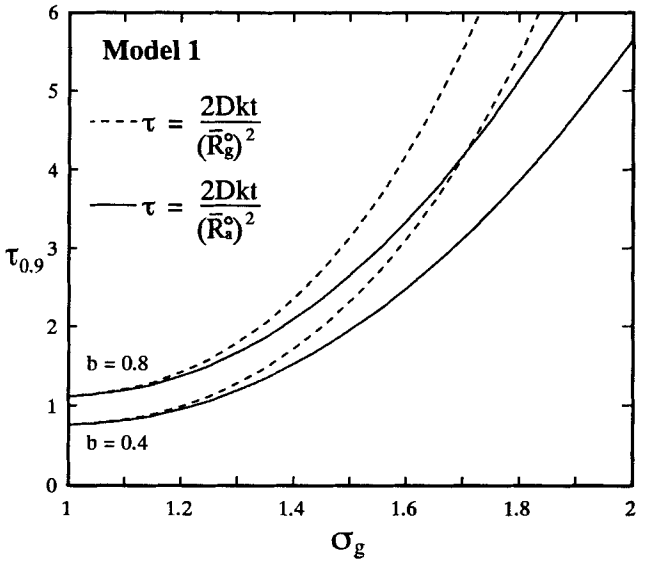

Fig. 12—The time $\tau_{0.9}$ to dissolve 90 pct of the initial volume fraction of particles is plotted as a function of σ_g after Model 1. The time τ is normalized against the arithmetic mean radius $\bar{R}_a^0$ (solid lines) and against the geometric mean radius $\bar{R}_g^0$ (dashed lines). The magnitude of the arithmetic mean radius is always greater than the geometric mean, and the difference increases with increasing value of σ_g.

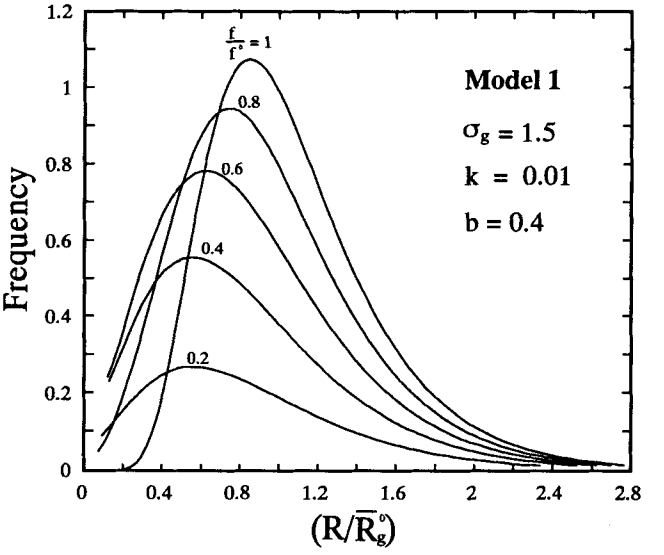

Fig. 13—The evolution of a particle size distribution with σ_g = 1.5 as the volume fraction of particles decreases. The radius of the small particles decreases at a higher rate than the radius of the large particles.

geometric mean radius, the arithmetic mean increases with increasing σ_g. Figure 12 clearly shows why the calculations done by Baty *et al.*[19] of the volume fraction of $CuAl_2$ against annealing time, assuming all particles of equal size ($\sigma_g \approx 1$), did not agree with the experimental observation. In Figure 13, the distribution of particles in space is shown for several values of the relative volume fraction f/f^0. As can be seen, the radius of the smaller particles decreases at a higher rate than the radius of the larger particles. Thus, the assumption made by Baty *et al.* that the particle distribution is moving rigidly to the left is not correct.

As discussed previously, Eq. [11] can be used to estimate the dissolution time for a particle of size R^0. In Model 1, the time τ^* to dissolve all of the particles in the material is identical to the time to dissolve the largest particle in the particle size distribution. This is due to the assumption in this model that there are no interactions between the particles.

For a given alloy, with an experimentally determined particle size distribution, the dissolution kinetics can be evaluated rather precisely from Figures 7 and 10. In general, the results are expected to lay in between the curves represented by Models 1 and 2. When only limited coarsening has taken place before up-quenching, Model 1 will describe the dissoluion rates most correctly, while after extensive coarsening, the dissolution

kinetics should approach the kinetics given by Model 2. Often it is more practical to estimate the time needed to dissolve a certain volume fraction of the particles. If one is satisfied with describing the dissolution process by giving the time needed to dissolve 90 pct of the initial volume fraction of particles, this can be obtained from the curves in Figure 12.

An equation for $\tau_{0.9}$ as a function of b and σ_g can be obtained from Figure 12 by curve fitting. One obtains

$$\tau_{0.9} \approx [0.3(1-b)^{-0.54} + 0.3(1 - 0.85 \ln \sigma_g)^{-4} + b^2(\sigma_g^2 - 1)] \left(\frac{0.01}{k}\right)^{0.05}$$

$$0 \le b \le 0.9 \quad 1 < \sigma_g \le 1.8 \qquad [12]$$

The deviation between the values predicted by Eq. [12] and the simulated values of $\tau_{0.9}$ is always less than 14 pct for the given ranges of b and σ_g.

To test the model, we have studied the dissolution kinetics of silicon particles in an Al-Si alloy. The results are presented in an accompanying article.[24]

APPENDIX A

Figure A1 shows a Dirichlet tessellation around points randomly distributed in a plane. If the points are assumed to be the center of particles that are nucleated simultaneously, the size of each particle is proportional to the size of the corresponding cell. A similar construction can be made for particles in space. In Model 1, this correspondence between the cell size and particle size is assumed to persist until the dissolution process starts. In addition, the following assumptions are made.

(1) Each particle is located at the center of the corresponding cell.
(2) The cells are assumed to be spherical.
(3) The cells are closed, *i.e.*, no solute is transferred between the cells.

As can be seen in Figure A1, the particles are often located near one of the boundaries of the cell. The same will be the case for particles in space. However, there is a tendency for the larger particles to be located near the center of the cell. This is a consequence of the growth process: a large particle is likely to have no close neighbors in order to grow big. If the particle has a close neighbor at one side, the probability for the particle to grow big will be reduced. In Figure A1, the large cells are also seen to be more circular than the small ones. In three dimensions, the larger cells will be rather spherical. This suggests that the assumptions in Model 1 are best satisfied for the larger particles. Because these particles also represent the majority of the volume fraction of particles, the assumptions in Model 1 are reasonable for dissolution of particles.

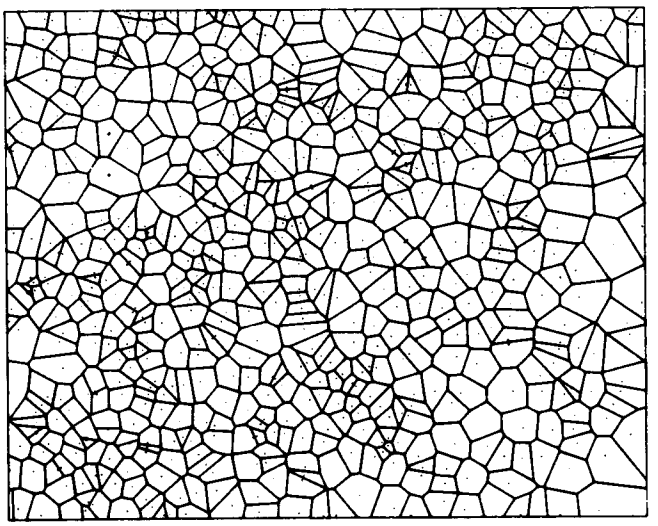

Fig. A1 — A random distribution of points in a plane, with the corresponding Dirichlet-tessellation.[25]

It is also worth noting that there is a correlation between the size of one particle (and its corresponding cell) and the size of its neighboring particles (cells). If the particle size is larger than the average, the distances to its nearest neighboring particles are likely to be larger than the average interparticle spacing. A consequence of this is that the nearest neighbors probably have no close neighbor in one direction. Thus, the probability for a neighboring particle to grow big is larger than random. The inverse is the case for a small particle and its neighboring particles. The tendency for large cells and the corresponding particles to cluster and small cells to do the same is clearly seen in Figure A1. If the particles are nucleated on a string and the diffusion occurs in one dimension, the correlation coefficient between the size of a particle and the size of its neighboring particles is 0.5. In two and three dimensions, the correlation is reduced by a factor of approximately 2 and 4, respectively. The effect of clustering is not included in our model.

APPENDIX B

In order to calculate the rate of dissolution of a spherical particle at the center of a sphere, it is convenient to use spherical coordinates. The concentration outside the particle is then a function of r and time only, and the calculations can thus be performed in one dimension. The solution method chosen for this linear transient problem (D independent of concentration) is a finite difference method, using a backward Euler time-integration method. This method is fully implicit and therefore we have no problems with numerical instability which can occur for other time-integration methods. The discretization method used closely follows the methods used by Patankar.[21] The boundary conditions for the present problem are

$$\nabla C(R_w, t) = 0 \qquad [B1]$$

and

$$C(R, t) = C^{\alpha/\beta} \qquad [B2]$$

where R_w is the radius of the cell and R is the radius of the particle. The N grid points are placed from the center of the particle to the cell wall, and each grid point is given a control volume that is shaped like a spherical shell. The number of grid points that are located inside the particle is k. The distance between each grid point can be varied so that the spacing is fine where the concentration gradients are steep and coarser where the concentration varies rather slowly. Control volume faces are

placed midway between the grid points. The first and last control volumes are consequently only half. If the particle/matrix interface had been fixed at all times, this would have been a very easily solved problem, but the moving interface makes the task more complicated.

Fick's first law in spherical coordinates gives the flux of atoms through a spherical surface:

$$J(r) = -\frac{D}{V_m}\frac{\partial C}{\partial r} \qquad [B3]$$

where V_m is the molar volume and D the diffusion coefficient. The concentrations that appear are in atomic percent. The mass balance for solute flow through the spherical shell in Figure B1 is given by

$$J_w A_w - J_e A_e = \frac{V}{V_m}\frac{\partial C}{\partial t} \qquad [B4]$$

where V is the volume of the shell and A_w and A_e are the area of the control volume faces at the inside and the outside, respectively. Equation [B4] can, after substitution of Fick's first law, be integrated over the control volume by assuming a piecewise linear profile for the concentration and by using a backward Euler time-integration method. The resulting equation takes the following form:

$$a_P C_P = a_W C_W + a_E C_E + a_P^0 C_P^0 \qquad [B5]$$

where C_P^0 is the concentration at point P at time t and C_P, C_W, and C_E are the concentrations at the actual grid-point at time $t + \Delta t$. The coefficients in front of the concentrations are given by

$$a_W = \frac{r_w^2}{r^2 \Delta r \delta r_w} \qquad [B6]$$

$$a_E = \frac{r_e^2}{r^2 \Delta r \delta r_e} \qquad [B7]$$

$$a_P^0 = \frac{1}{D\Delta t} \qquad [B8]$$

$$a_P = a_P^0 + a_W + a_E \qquad [B9]$$

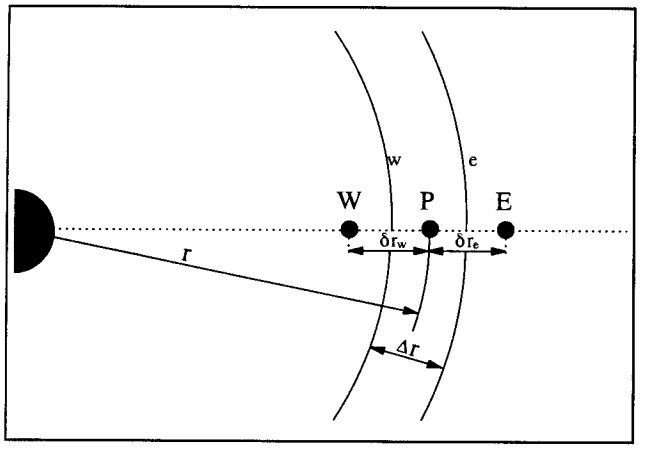

Fig. B1 — A 2-D model of a spherical cell at distance r from the center of a spherical particle.

There is one equation for each control volume. The N-k linear equations outside the particle are coupled equations. As a consequence, if one of the boundary concentrations is known, all of the equations can be solved, for instance, by the special algorithm called TriDiagonal-Matrix Algorithm.

For the last control volume, the boundary conditions of Eq. [B1] require that the amount of solute flowing into this control volume is accumulated. This causes a buildup of solute at the cell wall, causing the concentration gradients to level out, which again makes the dissolution rate of the particle slow down.

At the start of the dissolution process, the concentrations at grid points inside the particle are all equal to $C^{\beta/\alpha}$ and the concentrations outside the particle are all C_m. At the particle surface, the concentration is $C^{\alpha/\beta}$. To solve the equations, the concentration in at least one boundary point or the flux across the corresponding boundary has to be known. The problem is that the moving particle surface is never located exactly at a grid point, which means that no boundary concentrations are directly known. This problem has been solved by estimating the concentration at the grid point $k + 1$ just outside the particle/matrix interface at time $t + \Delta t$. The velocity of the interface is calculated from the previous iteration, and the location of the interface at time $t + \Delta t$ is calculated by assuming the velocity to be constant within the time interval $t - \Delta t$ to $t + \Delta t$. The concentration at the grid point $k + 1$ is then calculated by assuming the concentration gradient between the interface and grid point $k + 1$ at time $t + \Delta t$ to be the same as the gradient between grid points $k + 1$ and $k + 2$ at time t. The value of C_{k+1} is then used as a boundary value to solve the N-k equations for the other concentrations at time $t + \Delta t$.

This method to solve the moving interface problem is very accurate when the interface velocity is nearly constant within two time steps and when the concentration gradients used in the interpolation are approximately equal. The method does not require iterations within the time-step and thus is very fast. The number of grid points used in the calculations varied from 400 to about 700, with at least 100 grid points located inside the particle at the start of the dissolution process. Some runs with about 1000 grid points were also carried out, but there was almost nothing to gain in accuracy by this increase. The time step could be varied in order to adjust the radius reduction from iteration to iteration.

According to Whelan, the time τ^* to dissolve a very concentrated particle ($k \approx 0$) in an infinite matrix ($b \approx 0$) is very close to unity. This was used to test the accuracy of the numerical calculations in our model. One run with $k = 10^{-5}$ and $b = 10^{-3}$ gave the result $\tau^* = 0.9986$, which must be very close to the exact dissolution time.

In Model 1, we were able to reduce the overall computing time by almost a factor equal to the number of size classes without reducing the accuracy of the results. Calculations were carried out on one particle only, and the values of the relative radius ρ_1 as a function of normalized time τ_1 were stored in a table. The radius of a particle in size class i can be obtained by noting that the relative radius $\rho_i = \rho_1$ if $\tau_i = \tau_1$ (valid as long as b has the same value). Thus, the value of ρ_i was obtained by

a linear interpolation of the τ_1 values and the corresponding ρ_1 values. Five hundred size classes could be handled without increasing the computing time by a factor of 2 as compared to the computing time for dissolution of one particle.

In Model 2, the number of size classes and the number of grid points had to be reduced in order to avoid unrealistic long computing times. A number of 15 size classes and 150 to about 500 grid points were used at the start of the dissolution process, which means that the accuracy in the results obtained in this model were not quite as good as those obtained in Model 1.

The size of the particle was found from the difference between the total number of alloying atoms and the number of solute atoms in the matrix.

REFERENCES

1. G. Thomas and M.J. Whelan: *Phil. Mag.*, 1961, vol. 6, pp. 1103-14.
2. H.B. Aaron: *Met. Sci. J.*, 1968, vol. 2, pp. 192-98.
3. M.J. Whelan: *Met. Sci. J.*, 1969, vol. 3, pp. 95-97.
4. H.B. Aaron and G.R. Kotler: *Met. Sci. J.*, 1970, vol. 4, pp. 222-25.
5. F.V. Nolfi, P.G. Shewmon, and J.S. Foster: *Trans. AIME*, 1969, vol. 245, pp. 1427-33.
6. Frank V. Nolfi, Jr., Paul G. Shewmon, and James S. Foster: *Metall. Trans.*, 1970, vol. 1, pp. 789-800.
7. Frank V. Nolfi, Jr., Paul G. Shewmon, and James S. Foster: *Metall. Trans.*, 1970, vol. 1, pp. 2291-98.
8. S.N. Singh and M.C. Flemings: *Trans. AIME*, 1969, vol. 245, pp. 1803-09.
9. S.N. Singh and M.C. Flemings: *Trans. AIME*, 1969, vol. 245, pp. 1811-19.
10. S.N. Singh. B.P. Bardes, and M.C. Flemings: *Metall. Trans.*, 1970, vol. 1, pp. 1383-88.
11. E.G. Fuchs and A. Roósz: *Metall. Trans.*, 1972, vol. 3, pp. 1019-20.
12. R.A. Tanzilli and R.W. Heckel: *Trans. AIME*, 1968, vol. 242, pp. 2313-21.
13. J. Ågren: *J. Phys. Chem. Solids*, 1982, vol. 43, pp. 385-91.
14. J. Ågren: *Acta Metall.*, 1982, vol. 30, pp. 841-51.
15. J. Ågren: *Mater. Sci. Eng.*, 1982, vol. 55, pp. 135-41.
16. J. Ågren and G.P. Vassilev: *Mater. Sci. Eng.*, 1984, vol. 64, pp. 95-103.
17. J. Ågren, H. Abe, T. Suzuki, and Y. Sakuma: *Metall. Trans. A*, 1986, vol. 17A, pp. 617-20.
18. J. Ågren: *Scand. J. Metall.*, 1990, vol. 19, pp. 2-8.
19. D.L. Baty, R.A. Tanzilli, and R.W. Heckel: *Metall. Trans.*, 1970, vol. 1, pp. 1651-56.
20. E.E. Underwood: *Quantitative Sterelogy*, Addison-Wesley, Reading, MA, 1970, pp. 119-23.
21. S.W. Patankar: in *Numerical Heat Transfer and Fluid Flow*, M.A. Phillips and E.M. Millman, eds., Hemisphere, New York, NY, 1980.
22. H.E. Exner: *Int. Metall. Rev.*, 1972, vol. 17, pp. 25-42.
23. L.C. Brown: *Metall. Trans. A*, 1984, vol. 15A, pp. 449-58.
24. U.H. Tundal and N. Ryum: *Metall. Trans. A*, 1992, vol. 23A, pp. 445-49.
25. G. Burger, E. Koken, D.S. Wilkinson, and J.D. Embury: in *Advances in Phase Transitions*, J.D. Embury and G.R. Purdy, eds., Pergamon Press, New York, NY, 1988, p. 257.